


Speeding Up Entanglement Generation by Proximity to Higher-Order Exceptional Points

Zeng-Zhao Li^{1,2,*}, Weijian Chen^{1,3,†}, Maryam Abbasi^{1,3}, Kater W. Murch³, and K. Birgitta Whaley^{1,2,‡}

¹Department of Chemistry, University of California, Berkeley, California 94720, USA

²Berkeley Center for Quantum Information and Computation, Berkeley, California 94720, USA

³Department of Physics, Washington University, St. Louis, Missouri 63130, USA

 (Received 13 October 2022; revised 29 June 2023; accepted 1 August 2023; published 8 September 2023)

Entanglement is a key resource for quantum information technologies ranging from quantum sensing to quantum computing. Conventionally, the entanglement between two coupled qubits is established at the timescale of the inverse of the coupling strength. In this Letter, we study two weakly coupled non-Hermitian qubits and observe entanglement generation at a significantly shorter timescale by proximity to a higher-order exceptional point. We establish a non-Hermitian perturbation theory based on constructing a biorthogonal complete basis and further identify the optimal condition to obtain the maximally entangled state. Our study of speeding up entanglement generation in non-Hermitian quantum systems opens new avenues for harnessing coherent nonunitary dissipation for quantum technologies.

DOI: [10.1103/PhysRevLett.131.100202](https://doi.org/10.1103/PhysRevLett.131.100202)

Introduction.—Since the discovery of their real spectra, parity-time (\mathcal{PT}) symmetric Hamiltonians [1,2] a special class of non-Hermitian Hamiltonians have been intensively studied in the past two decades [3–5]. One intriguing feature of such \mathcal{PT} -symmetric non-Hermitian systems is the nontrivial degeneracy known as the exceptional point (EP) where both eigenenergies and eigenstates coalesce. This unique feature has been experimentally demonstrated in many classical systems [6–8] with applications such as wave transport control [9–12], laser emission management [13–15], and enhanced sensing [16–18]. Recently, various approaches such as dissipation engineering [19] and Hamiltonian dilation [20] have been utilized to study non-Hermitian physics in quantum systems [21,22]. EPs have been observed in various quantum platforms such as the nitrogen-vacancy color center [20], trapped ions [23,24], ultracold atoms [25], and superconducting circuits [19], and offer new possibilities in quantum applications such as sensing [26] and state control [27,28]. Although the majority of detailed studies focus on single spin or spin ensembles described in Hilbert space with dimension $N = 2$, there are several pioneering works studying the coherence and entanglement in a larger Hilbert space [29,30]. A very recent work demonstrates entanglement between one effective non-Hermitian qubit and one Hermitian qubit that achieves the maximum allowed value at the EP [31].

In this Letter, we study the entanglement generation between two driven non-Hermitian qubits that are weakly coupled. In the absence of coupling, the two-qubit system exhibits a fourth-order EP. The weak coupling is a perturbation, lifting the degeneracy and altering the two-qubit dynamics. We observe a characteristic pattern of phase accumulation among the basis states, which lead to a

maximally entangled state at a timescale much shorter than the inverse of the coupling strength. We further observe that by approaching the EP, a weaker coupling strength is needed to establish the maximally entangled state, at the cost of longer buildup time. In addition, we develop a non-Hermitian perturbation theory and use this to obtain analytical solutions of the concurrence evolution, which agrees well with the numerical simulations.

The model.—The system under consideration consists of two coupled driven non-Hermitian qubits, where the lower energy level has energy dissipation out of the qubit manifold, $\{|e\rangle, |f\rangle\}$, as shown in Fig. 1(a). Such a non-Hermitian qubit has been realized in a transmon superconducting circuit [19]. The Hamiltonian (setting $\hbar = 1$) for a single non-Hermitian qubit is given by

$$H_{j=1,2} = \left(\Delta_j - \frac{i\gamma_j}{2} \right) \sigma_j^- \sigma_j^+ + \Omega_j \sigma_j^x, \quad (1)$$

where Δ_j represents frequency detuning of the applied drive from the qubit transition frequency, γ_j denotes the energy decay rate of $|e\rangle_j$, and Ω_j is the drive amplitude. The Pauli operators are defined in terms of energy levels $|e\rangle_j$ and $|f\rangle_j$ as $\sigma_j^+ = |f\rangle_j \langle e|$, $\sigma_j^- = |e\rangle_j \langle f|$, and $\sigma_j^x = |f\rangle_j \langle e| + |e\rangle_j \langle f|$ ($j = 1, 2$). The eigenvalues of $H_j(\Delta_j = 0)$ are given by $\lambda_{j,\pm} = (-i\gamma_j \pm \eta_j)/4$, with $\eta_j \equiv \sqrt{16\Omega_j^2 - \gamma_j^2}$, and there exists a second-order EP when $\Omega_j = \gamma_j/4$.

The coupled non-Hermitian qubits are then described by the Hamiltonian

$$H = \sum_{j=1,2} H_j + J(\sigma_1^+ \sigma_2^- + \sigma_1^- \sigma_2^+), \quad (2)$$

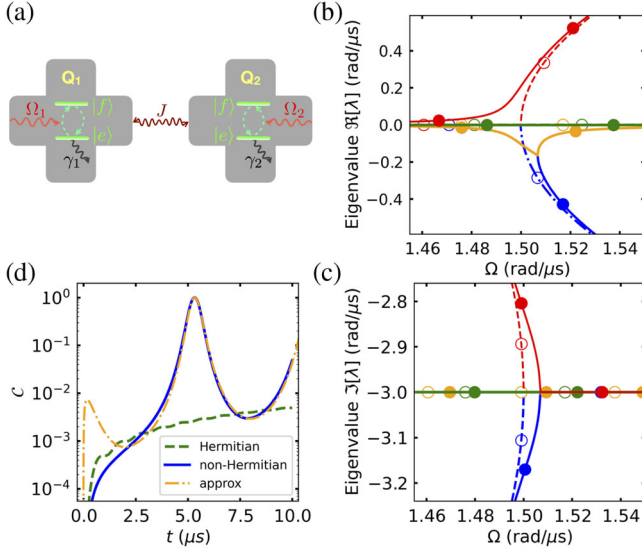


FIG. 1. (a) Schematic of two coupled non-Hermitian qubits with coupling J . The lower level of each qubit has energy dissipation $\gamma_{j=1,2}$ and the two levels of each qubit are coupled by a drive $\Omega_{j=1,2}$. (b),(c) Real (b) and imaginary (c) parts of the eigenvalues for $J = 0$ (dashed curves with empty circles) and for $J = 0.001$ rad/ μ s (solid curves with full circles). The two qubits are assumed to have the same drive amplitude Ω and the same decay rates $\gamma_{1,2} = 6 \mu\text{s}^{-1}$. The circles are visual aids to distinguish the solid and dashed lines. (d) Concurrence evolution of the coupled non-Hermitian qubits near the fourth-order EP (solid blue curve). The yellow dashed curve shows the perturbative analytical result calculated with Eq. (3) [33]. The initial state is $|ff\rangle$ and other parameters used are $\gamma_{1,2} = 6 \mu\text{s}^{-1}$, $\Omega_{1,2} = 1.6$ rad/ μ s, $\Delta_{1,2} = 0$, and $J = 0.001$ rad/ μ s. The dashed green curve shows the concurrence evolution for two coupled Hermitian qubits with the same coupling J , also with the initial state $|ff\rangle$.

where J denotes the effective coupling strength between the two qubits. When the drives are resonant with both qubits, i.e., $\Delta_j = 0$, Eq. (2) reduces to a so-called passive \mathcal{PT} -symmetric Hamiltonian [32] that can be further written as $H(\Delta_j = 0) = H_{\mathcal{PT}} - (i\gamma_1/4) - (i\gamma_2/4)$, where the Hamiltonian $H_{\mathcal{PT}}$ respects \mathcal{PT} -symmetry, i.e., $\mathcal{P}T H_{\mathcal{PT}} (\mathcal{P}T)^{-1} = H_{\mathcal{PT}}$ with parity operator $\mathcal{P} = \sigma_1^x \sigma_2^x$ and T the time reversal operator (equivalent to complex conjugation).

We restrict our attention to the resonant case and assume the Hamiltonians for the two qubits are identical, i.e., $\Delta_1 = \Delta_2 = 0$, $\gamma_1 = \gamma_2 = \gamma$, and $\Omega_1 = \Omega_2 = \Omega$. In the absence of qubit coupling (i.e., $J = 0$), each qubit in its Hilbert space with dimension $N = 2$ exhibits a second-order EP, while the two-qubit system described by the Hamiltonian in Eq. (2) with a Hilbert space with dimension $N = 4$ exhibits a fourth-order EP at $\Omega = \Omega_{\text{EP}} \equiv (\gamma/4)$ [see Figs. 1(b) and 1(c) and Fig. S1(a) in [33]]. The weak coupling J between the two qubits acts as a perturbation, lifting the degeneracy and lowering the order of the EP

[e.g., to a second-order EP at a shifted position in Figs. 1(b) and 1(c)] [33].

The two-qubit evolution can be solved from the Hamiltonian in Eq. (2), and the normalized quantum state has a general form $|\tilde{\psi}\rangle = (|\psi\rangle/||\psi\rangle|) = \alpha|ff\rangle + \beta|fe\rangle + \zeta|ef\rangle + \delta|ee\rangle$, where the state $|\psi\rangle$ is normalized conventionally. We use the concurrence \mathcal{C} [41] to quantify the entanglement between the two qubits, which is given by $\mathcal{C} = 2|\alpha\delta - \beta\zeta|$. Conventionally, two qubits with dipolar coupling as in Eq. (2) and initialized in the state $|fe\rangle$ (or $|ef\rangle$) will generate Bell states on a timescale of $1/J$. Here, we find that by ensuring proximity to the fourth-order EP, weakly coupled non-Hermitian qubits ($J \ll \gamma$) with initial state $|ff\rangle$ can have entanglement generation on a timescale much shorter than $1/J$. Figure 1(d) shows an example of this EP-enhanced entanglement generation, together with a comparison to the Hermitian case.

Non-Hermitian perturbation theory.—We construct a biorthogonal complete basis from the states in both the Hilbert and corresponding dual spaces of the two qubits and extend the standard perturbation theory of Hermitian quantum mechanics to develop a time-independent perturbation theory for non-Hermitian systems [33]. In addition, we also generalize standard degenerate perturbation theory to deal with the existence of non-Hermitian degeneracies [33].

With perturbative eigenstates $|\Psi_j\rangle$ and eigenvalues Λ_j for $\Omega > \Omega_{\text{EP}}$ [33], we can obtain the state evolution $|\tilde{\psi}(t)\rangle = (|\psi(t)\rangle/||\psi(t)\rangle|)$, where $|\psi(t)\rangle = \sum_{j=++,-,-,1,2} \langle\tilde{\Psi}_j|\psi(0)\rangle \cdot e^{-it\Lambda_j} |\Psi_j\rangle$, with $\langle\tilde{\Psi}_{++}|, \langle\tilde{\Psi}_{--}|, \langle\tilde{\Psi}_1|, \langle\tilde{\Psi}_2|$ the corresponding left eigenstates in the biorthogonal basis. The use of a biorthogonal basis is crucial here since the Hamiltonian Eq. (2) is not in general \mathcal{PT} -symmetric, so the usual \mathcal{CPT} norm for \mathcal{PT} -symmetric Hamiltonians [42,43] does not apply. For the initial state $|\psi(0)\rangle = |ff\rangle$, the time evolution of concurrence is then given by [33]

$$\mathcal{C} = \left| \frac{16\eta^2\Omega^2(e^{it\chi_2} - 1)}{\mathcal{B}} \right|, \quad (3)$$

where $\mathcal{B} = 16\Omega^2(\gamma^2 + 32\Omega^2) + \gamma\{\gamma(\gamma^2 - \eta^2)\cos(\eta\eta) - 2\gamma^2\eta\sin(\eta\eta) - 64\Omega^2\cos(t\chi_2/2)[\gamma\cos(\eta\eta/2) - \eta\sin(\eta\eta/2)]\}$ and $\chi_2 = J[(\eta^2 + 3\gamma^2)/\eta^2]$. The analytical result from Eq. (3) agrees well with the numerical simulation results in Fig. 1(d) (except for the region close to $t = 0$ [33]). In the following sections we discuss the mechanism of entanglement generation in detail and show how the entanglement generation is enhanced by approaching the fourth-order EP.

Entanglement generation near the EP.—We first examine the complex amplitudes of $|\tilde{\psi}(t)\rangle$ at each basis state in the absence of the qubit coupling, i.e., $J = 0$ [Figs. 2(a) and 2(b)]. The qubit drive is chosen as $\Omega = 1.6$ rad/ μ s, which places the system in the regime of \mathcal{PT} -symmetry preserving phase. The two qubits evolve independently; therefore the two-qubit state evolves successively through states

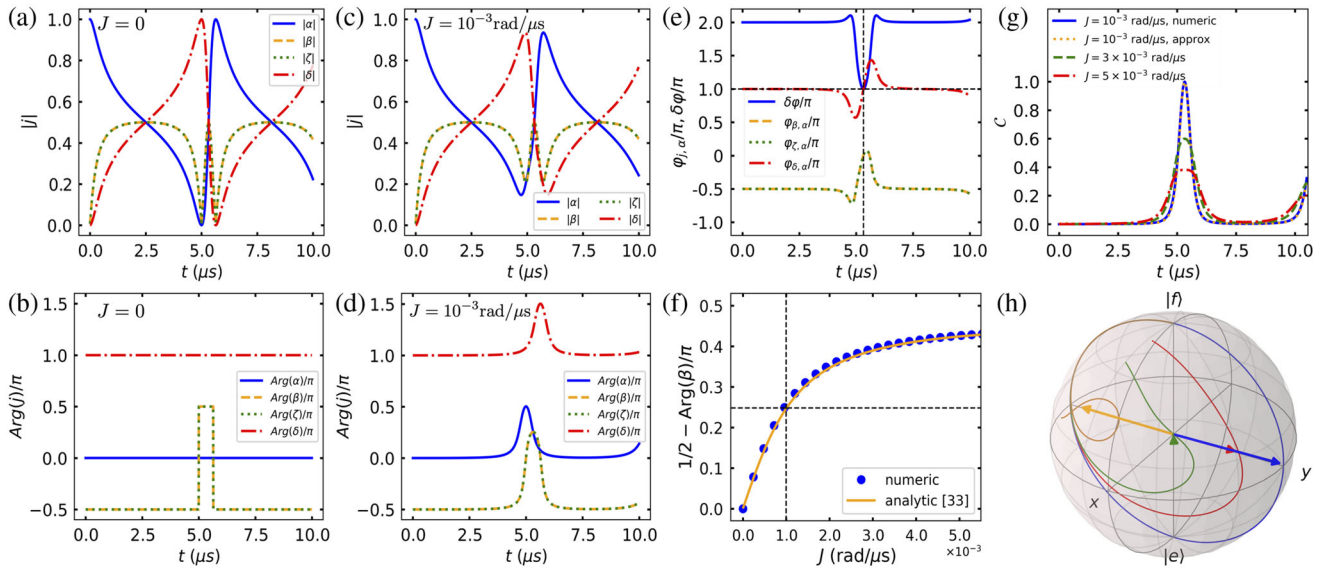


FIG. 2. (a)–(d) Time evolution of the modulus $|j|$ and the angle $\text{Arg}(j)$ ($j = \alpha, \beta, \zeta, \delta$) for each of the four complex amplitudes of the two-qubit state $|\tilde{\psi}\rangle = \alpha|ff\rangle + \beta|fe\rangle + \zeta|ef\rangle + \delta|ee\rangle$ for $J = 0$ (a),(b) and $J = 10^{-3}$ rad/ μs (c),(d). (e) Time evolution of the phase relative to basis state $|ff\rangle$, i.e., $\varphi_{j,\alpha} \equiv \text{Arg}(j) - \text{Arg}(\alpha)$ for ($j = \beta, \zeta, \delta$) and of $\delta\varphi \equiv \text{Arg}(\alpha) + \text{Arg}(\delta) - \text{Arg}(\beta) - \text{Arg}(\zeta)$ for $J = 10^{-3}$ rad/ μs . The value $\delta\varphi = \pi$ at $t = T_0^* = 5.325$ μs signifies maximal entanglement. (f) Dependence on J of $\text{Arg}(\beta)$ relative to its value for $J = 0$ [panel (b)], i.e., the differential phase $\pi/2 - \text{Arg}(\beta)$, at time $t = 5.325$ μs . (g) Examples of concurrence for $J = 10^{-3}$, 3×10^{-3} , 5×10^{-3} rad/ μs . Maximal concurrence generation ($\mathcal{C} = 1$) is observed at $t = 5.325$ μs for $J = 10^{-3}$ rad/ μs , with the values from Eq. (3) (orange dotted curve) in good agreement with the full numerical calculation (blue solid curve). (h) Trajectories of reduced single qubit dynamics on the reduced qubit Bloch sphere for $J = 0$ (blue), 5×10^{-4} (red), 10^{-3} (green), 5×10^{-3} rad/ μs (orange) with evolution time between 0 and $t = 4\pi/\eta = 5.64$ μs (i.e., a single period for decoupled qubits with $J = 0$). Arrows point to the reduced qubit states at time $t = 5.325$ μs , with the blue arrow pointing to $|+\rangle + |y\rangle$, the green arrow pointing to the origin (indicating a maximally entangled state), and the red and orange arrows aligning with the $\pm y$ axis. Unless otherwise specified, all plots are made for $|\psi(0)\rangle = |ff\rangle$, $\Omega = 1.6$ rad/ μs , and $\gamma = 6$ μs^{-1} .

$|ff\rangle$, $(|f\rangle - |e\rangle) \otimes (|f\rangle - |e\rangle)$, $|ee\rangle$, and $(|f\rangle + |e\rangle) \otimes (|f\rangle + |e\rangle)$, returning to $|ff\rangle$ after one period (i.e., $t = 4\pi/\eta \sim 5.64$ μs). An interesting feature is the distorted Rabi-like oscillation of the population of $|ee\rangle$ and $|ff\rangle$ states, shown as the blue and red curves in Fig. 2(a). Inspection of the behavior shortly before 5.64 μs reveals that at the time $t = T_0^* = 5.325$ μs all basis states have equal amplitude. Figure 2(b) shows that the phases of the $|ef\rangle$ and $|fe\rangle$ states experience sudden jumps of π , corresponding to the state of one of the two qubits passing through a pole of the corresponding qubit Bloch sphere. When all basis amplitudes are equal, the concurrence, $\mathcal{C} = 2|\alpha\delta - \beta\zeta|$, can be shown to be equal to $|\sin(\delta\varphi/2)|$ with $\delta\varphi \equiv \text{Arg}(\alpha) + \text{Arg}(\delta) - \text{Arg}(\beta) - \text{Arg}(\zeta)$. Evaluating the phase $\delta\varphi$ at T_0^* it is evident that concurrence \mathcal{C} is identically equal to zero. This is consistent with evaluation of Eq. (3) with $J = 0$.

Figures 2(c) and 2(d) now summarize the state evolution with a finite but weak coupling strength ($J = 10^{-3}$ rad/ μs). The populations of the basis states in Fig. 2(c) exhibit a similar distorted oscillatory behavior, but with reduced visibility relative to that for $J = 0$. Here, the two-qubit state does not return to the product states $|ff\rangle$ and $|ee\rangle$ because of the qubit coupling. Also, while at the time T_0^* we still observe that $|\alpha| \sim |\beta| \sim |\zeta| \sim |\delta|$, Fig. 2(d) shows that the

phase evolution of each basis state is now significantly altered near T_0^* . In particular, the π phase jumps of $\text{Arg}(\beta)$ and $\text{Arg}(\zeta)$ that are seen for $J = 0$ in Fig. 2(b), now become Gaussian-shape profiles with significantly reduced phase contrast. Physically speaking, we can intuitively understand this effect as a result of the weak qubit-qubit coupling J pulling the qubit dynamics away from the poles of the Bloch sphere, so that no discrete π phase jumps occur.

The time evolution of the relative phases with respect to that of basis state $|ff\rangle$, i.e., $\varphi_{j,\alpha} \equiv \text{Arg}(j) - \text{Arg}(\alpha)$ ($j = \beta, \zeta, \delta$), is shown for coupling strength $J = 10^{-3}$ rad/ μs in Fig. 2(e), together with the phase $\delta\varphi$ (solid blue line). At T_0^* where the populations at each basis state are still approximately equal, the relative phase $\varphi_{\delta,\alpha}$ is still equal to π , as in Fig. 2(b) for $J = 0$, but the values of $\varphi_{\beta,\alpha}$ and $\varphi_{\zeta,\alpha}$ are now no longer equal to $\pi/2$. In fact, the state is very close to $|\tilde{\psi}\rangle = e^{i(\pi/4)}(|ff\rangle + |fe\rangle + |ef\rangle + e^{+i\pi}|ee\rangle)/2$, which has $\delta\varphi = \pi$ and $\mathcal{C} = 1$.

Figure 2(f) now shows the change in phase of $\text{Arg}(\beta)$ relative to its value at $J = 0$, i.e., the differential phase $\pi/2 - \text{Arg}(\beta)$, as a function of the coupling strength J . The analytical results [Eq. (S77) in [33]] agree well with the full numerical results. At a given drive amplitude Ω , there exists

an optimal coupling strength J to satisfy the condition $\delta\varphi = \pi$ that realizes the maximally entangled state on a timescale $1/\eta (\ll 1/J)$. This change in differential phase of $|fe\rangle$ and $|ef\rangle$ can be understood as a consequence of the degeneracy lifting by a finite J value (with $J \ll \Omega$). Figure 2(g) shows that further increase of J does not benefit the entanglement generation. The analytical expression from Eq. (3) for $J = 10^{-3}$ rad/ μs shows good agreement with the numerical simulations.

To get more physical intuition into this enhancement of entanglement, we also calculate the reduced single qubit dynamics, i.e., after tracing out one of the two qubits. Figure 2(h) shows the trajectories of the reduced qubit dynamics on the corresponding Bloch sphere during one period $4\pi/\eta = 5.64 \mu\text{s}$. For $J = 0$, the reduced qubit evolves on the surface of the Bloch sphere, while for nonzero J , the reduced qubit dynamics lie inside the Bloch sphere, suggesting possible entanglement generation. Only at a specific value of J will the qubit trajectory pass through the origin where the reduced qubit is in a fully mixed state, implying that two qubits are in a maximally entangled state. It is then evident that for a given value of Ω , maximum entanglement will occur at a specific time T^* and for a specific coupling strength J^* .

EP enhanced entanglement generation.—Next, we study the differential phase of the $|ef\rangle$ and $|fe\rangle$ states relative to their $J = 0$ values, i.e., $\pi/2 - \text{Arg}(\beta)$ at T^* , for different values of the drive amplitude Ω [Fig. 3(a)]. On approaching the EP, the slope of the phase change gets sharper, and therefore a smaller coupling strength is needed to achieve the maximally entangled state. The increasingly sharp change in differential phase on approaching the EP [Fig. 3(a)] suggests that the entanglement generation near the EP can provide a sensitive measure of the magnitude of the qubit coupling J [44]. The density plot of concurrence versus Ω and t in Fig. 3(b) shows how the optimal parameters $\{\Omega^*, T^*\} = \{1.6 \text{ rad}/\mu\text{s}, 5.325 \mu\text{s}\}$ can be identified for a given qubit coupling J . For this example with $J = 10^{-3}$ rad/ μs , the maximal concurrence $\mathcal{C} = 1$ corresponds to the peak of the blue curve in Fig. 2(g). Figure 3(c) shows the entanglement enhancement for non-Hermitian qubits relative to their corresponding Hermitian qubits. It is evident that non-Hermitian qubits can be entangled significantly faster than Hermitian qubits, with the relative speedup increasing significantly as the perturbation J is decreased and the fourth-order EP at $J = 0$ is approached. The mixed power-law dependence, i.e., a combination of inverse cube root and fourth root, reflects the changing order of the EP as J decreases.

Discussion.—Throughout this Letter, we have focused on the case of two non-Hermitian qubits with identical Hamiltonian parameters, which may be challenging to realize in experiments. However, our mechanism is robust

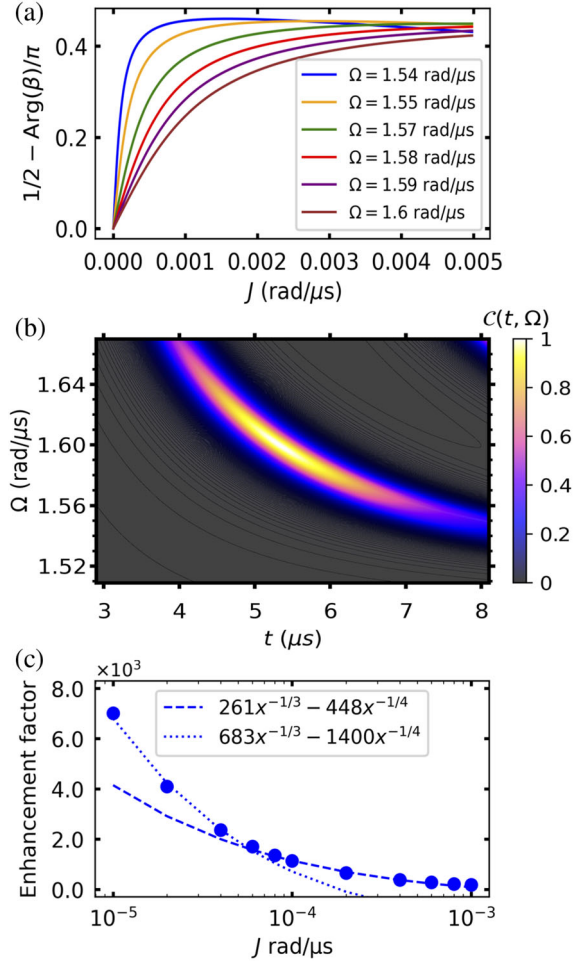


FIG. 3. (a) Phase of β relative to the corresponding value for $J = 0$, i.e., $\pi/2 - \text{Arg}(\beta)$, at different Ω values. The increased slope on approaching the EP at $\Omega_{\text{EP}} = 1.5$ rad/ μs indicates the enhancement due to proximity to the EP. (b) Density plot of concurrence as a function of drive amplitude Ω and time t , with J fixed at 10^{-3} rad/ μs . Identification of the maximal concurrence $\mathcal{C} = 1$ yields the optimal parameters $(\Omega^*, T^*) = (1.6 \text{ rad}/\mu\text{s}, 5.325 \mu\text{s})$. (c) Entanglement enhancement factor defined as the ratio of the first time to achieve maximal entanglement for the Hermitian case ($\sim 1/J$) to the corresponding time T^* for the non-Hermitian case (see also Fig. S2 in [33]).

with respect to the parameter values and still holds when the qubit parameters differ within a small range. In Fig. 4, we compare the concurrence evolution for fixed $\gamma_1 = 6 \mu\text{s}^{-1}$ and variable $\gamma_2 = 5, 7 \mu\text{s}^{-1}$. The concurrence degrades significantly if both Ω_1 and Ω_2 are maintained at 1.6 rad/ μs , as chosen in Fig. 2. However, if Ω_2 is adjusted to ensure the two qubits have the same period, i.e., $16\Omega_1^2 - \gamma_1^2 = 16\Omega_2^2 - \gamma_2^2$, an entangled state with concurrence $\mathcal{C} \approx 1$ is regained. We further note that our method still provides an advantage for relatively large J values. For example, for $J = 0.1$ rad/ μs , the maximally entangled state can be obtained in less than 2 μs , while it takes about 8 μs for Hermitian qubits to reach this state (see Fig. S4 in [33]).

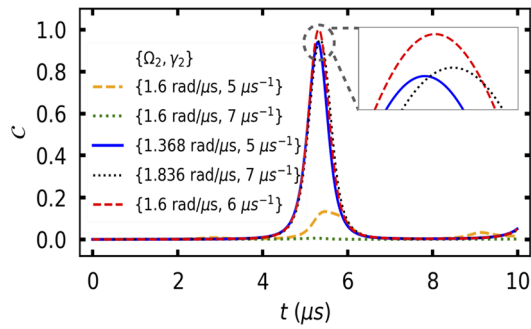


FIG. 4. Time evolution of concurrence for two qubits with different Hamiltonian parameters. $\{\Omega_1, \gamma_1\} = \{1.6 \text{ rad}/\mu\text{s}, 6 \mu\text{s}^{-1}\}$ are fixed, while the parameters of the second qubit take on the values shown in the legend. The red dashed curve for $\{\Omega_2, \gamma_2\} = \{\Omega_1, \gamma_1\}$ is included as a reference. The initial state and coupling strength are given by $|\psi(0)\rangle = |ff\rangle$ and $J = 10^{-3} \text{ rad}/\mu\text{s}$, respectively, for all calculations.

More detailed discussion on the effects of a nonresonant qubit drive, of decoherence, and of the entanglement generation in the Hermitian limit is given in [33].

Conclusions.—We have studied the entanglement between two weakly coupled non-Hermitian qubits that can be generated at a speed much faster than the inverse of the interqubit interaction, by forcing proximity to a higher-order exceptional point. This demonstrates a fundamentally new and advantageous entanglement generation method, which offers considerable potential for applications in quantum information science and technology, including the sensing of weak coupling between qubits and common two-level system impurities or defects.

This work has been supported by AFOSR MURI Grant No. FA9550-21-1-0202. We are grateful to Philippe Lewalle and Rob Cook for helpful discussions.

Z.-Z. L. and W. C. contributed equally to this work.

*zengzhaoli09@gmail.com

†wchen34@wustl.edu

*whaley@berkeley.edu

- [1] C. M. Bender and S. Boettcher, Real Spectra in Non-Hermitian Hamiltonians having \mathcal{PT} Symmetry, *Phys. Rev. Lett.* **80**, 5243 (1998).
- [2] C. M. Bender, Making sense of non-Hermitian Hamiltonians, *Rep. Prog. Phys.* **70**, 947 (2007).
- [3] R. El-Ganainy, K. G. Makris, M. Khajavikhan, Z. H. Musslimani, S. Rotter, and D. N. Christodoulides, Non-Hermitian physics and \mathcal{PT} symmetry, *Nat. Phys.* **14**, 11 (2018).
- [4] Ş. K. Özdemir, S. Rotter, F. Nori, and L. Yang, Parity-time symmetry and exceptional points in photonics, *Nat. Mater.* **18**, 783 (2019).
- [5] Y. Ashida, Z. Gong, and M. Ueda, Non-Hermitian physics, *Adv. Phys.* **69**, 249 (2020).

- [6] C. Dembowski, H. D. Gräf, H. L. Harney, A. Heine, W. D. Heiss, H. Rehfeld, and A. Richter, Experimental Observation of the Topological Structure of Exceptional Points, *Phys. Rev. Lett.* **86**, 787 (2001).
- [7] H. Hodaei, Mohammad-Ali Miri, M. Heinrich, D. N. Christodoulides, and M. Khajavikhan, Parity-time-symmetric microring lasers, *Science* **346**, 975 (2014).
- [8] H. Xu, D. Mason, L. Jiang, and J. G. E. Harris, Topological energy transfer in an optomechanical system with exceptional points, *Nature (London)* **537**, 80 (2016).
- [9] C. E. Rüter, K. G. Makris, R. El-Ganainy, D. N. Christodoulides, M. Segev, and D. Kip, Observation of parity-time symmetry in optics, *Nat. Phys.* **6**, 192 (2010).
- [10] J. Doppler, A. A. Mailybaev, J. Böhm, U. Kuhl, A. Girschik, F. Libisch, T. J. Milburn, P. Rabl, N. Moiseyev, and S. Rotter, Dynamically encircling an exceptional point for asymmetric mode switching, *Nature (London)* **537**, 76 (2016).
- [11] Y. Choi, C. Hahn, J. W. Yoon, S. H. Song, and P. Berini, Extremely broadband, on-chip optical nonreciprocity enabled by mimicking nonlinear anti-adiabatic quantum jumps near exceptional points, *Nat. Commun.* **8**, 14154 (2017).
- [12] X. L. Zhang, S. Wang, B. Hou, and C. T. Chan, Dynamically Encircling Exceptional Points: *In Situ* Control of Encircling Loops and the Role of the Starting Point, *Phys. Rev. X* **8**, 021066 (2018).
- [13] M. Brandstetter, M. Liertzer, C. Deutsch, P. Klang, J. Schöberl, H. E. Türeci, G. Strasser, K. Unterrainer, and S. Rotter, Reversing the pump dependence of a laser at an exceptional point, *Nat. Commun.* **5**, 4034 (2014).
- [14] B. Peng, S. K. Özdemir, M. Liertzer, W. Chen, J. Kramer, H. Yilmaz, J. Wiersig, S. Rotter, and L. Yang, Chiral modes and directional lasing at exceptional points, *Proc. Natl. Acad. Sci. U.S.A.* **113**, 6845 (2016).
- [15] Z. J. Wong, Y. L. Xu, J. Kim, K. O'Brien, Y. Wang, L. Feng, and X. Zhang, Lasing and anti-lasing in a single cavity, *Nat. Photonics* **10**, 796 (2016).
- [16] J. Wiersig, Enhancing the Sensitivity of Frequency and Energy Splitting Detection by Using Exceptional Points: Application to Microcavity Sensors for Single-Particle Detection, *Phys. Rev. Lett.* **112**, 203901 (2014).
- [17] W. Chen, Ş. K. Özdemir, G. Zhao, J. Wiersig, and L. Yang, Exceptional points enhance sensing in an optical microcavity, *Nature (London)* **548**, 192 (2017).
- [18] H. Hodaei, A. U. Hassan, S. Wittek, H. Garcia-Gracia, R. El-Ganainy, D. N. Christodoulides, and M. Khajavikhan, Enhanced sensitivity at higher-order exceptional points, *Nature (London)* **548**, 187 (2017).
- [19] M. Naghiloo, M. Abbasi, Y. N. Joglekar, and K. W. Murch, Quantum state tomography across the exceptional point in a single dissipative qubit, *Nat. Phys.* **15**, 1232 (2019).
- [20] Y. Wu, W. Liu, J. Geng, X. Song, X. Ye, C. K. Duan, X. Rong, and J. Du, Observation of parity-time symmetry breaking in a single-spin system, *Science* **364**, 878 (2019).
- [21] P. Lewalle and K. B. Whaley, Pontryagin-optimal control of a non-Hermitian qubit, *Phys. Rev. A* **107**, 022216 (2023).

- [22] Z. Z. Li, J. Atalaya, and K. B. Whaley, Topological quantum interference in a pumped Su-Schrieffer-Heeger lattice, *Phys. Rev. A* **105**, 052418 (2022).
- [23] L. Ding, K. Shi, Q. Zhang, D. Shen, X. Zhang, and W. Zhang, Experimental Determination of \mathcal{PT} -Symmetric Exceptional Points in a Single Trapped Ion, *Phys. Rev. Lett.* **126**, 083604 (2021).
- [24] W. C. Wang, Y. L. Zhou, H. L. Zhang, J. Zhang, M. C. Zhang, Y. etae, C. W. Wu, T. Chen, B. Q. Ou, W. Wu, H. Jing, and P. X. Chen, Observation of \mathcal{PT} -symmetric quantum coherence in a single-ion system, *Phys. Rev. A* **103**, L020201 (2021).
- [25] J. Li, A. K. Harter, J. Liu, L. de Melo, Y. N. Joglekar, and L. Luo, Observation of parity-time symmetry breaking transitions in a dissipative Floquet system of ultracold atoms, *Nat. Commun.* **10**, 855 (2019).
- [26] S. Yu *et al.*, Experimental Investigation of Quantum-Enhanced Sensor, *Phys. Rev. Lett.* **125**, 240506 (2020).
- [27] W. Liu, Y. Wu, C. K. Duan, X. Rong, and J. Du, Dynamically Encircling an Exceptional Point in a Real Quantum System, *Phys. Rev. Lett.* **126**, 170506 (2021).
- [28] M. Abbasi, W. Chen, M. Naghiloo, Y. N. Joglekar, and K. W. Murch, Topological Quantum State Control through Exceptional-Point Proximity, *Phys. Rev. Lett.* **128**, 160401 (2022).
- [29] J. Wen, C. Zheng, Z. Ye, T. Xin, and G. Long, Stable states with nonzero entropy under broken PT symmetry, *Phys. Rev. Res.* **3**, 013256 (2021).
- [30] A. Gautam, K. Dorai, and Arvind, Experimental demonstration of the dynamics of quantum coherence evolving under a PT-symmetric Hamiltonian on an NMR quantum processor, [arXiv:2201.05083](https://arxiv.org/abs/2201.05083).
- [31] A. Kumar, K. W. Murch, and Y. N. Joglekar, Maximal quantum entanglement at exceptional points via unitary and thermal dynamics, *Phys. Rev. A* **105**, 012422 (2022).
- [32] A. Guo, G. J. Salamo, D. Duchesne, R. Morandotti, M. Volatier-Ravat, V. Aimez, G. A. Siviloglou, and D. N. Christodoulides, Observation of \mathcal{PT} -Symmetry Breaking in Complex Optical Potentials, *Phys. Rev. Lett.* **103**, 093902 (2009).
- [33] See Supplemental Material at <http://link.aps.org/supplemental/10.1103/PhysRevLett.131.100202> for additional figures, theory development, and a detailed discussion on the effects of a nonresonant qubit drive, decoherence, and entanglement generation in the Hermitian limit, including citation of Refs. [33–39].
- [34] K. Petermann, Calculated spontaneous emission factor for double-heterostructure injection lasers with gain-induced waveguiding, *IEEE J. Quantum Electron.* **15**, 566 (1979).
- [35] M. V. Berry, Mode degeneracies and the Petermann excess-noise factor for unstable lasers, *J. Mod. Opt.* **50**, 63 (2003).
- [36] S. Y. Lee, J. W. Ryu, J. B. Shim, S. B. Lee, S. W. Kim, and K. An, Divergent Petermann factor of interacting resonances in a stadium-shaped microcavity, *Phys. Rev. A* **78**, 015805 (2008).
- [37] M. C. Zheng, D. N. Christodoulides, R. Fleischmann, and T. Kottos, \mathcal{PT} optical lattices and universality in beam dynamics, *Phys. Rev. A* **82**, 010103(R) (2010).
- [38] J. Majer *et al.*, Coupling superconducting qubits via a cavity bus, *Nature (London)* **449**, 443 (2007).
- [39] W. K. Wootters, Entanglement of Formation of an Arbitrary State of Two Qubits, *Phys. Rev. Lett.* **80**, 2245 (1998).
- [40] W. Chen, M. Abbasi, Y. N. Joglekar, and K. W. Murch, Quantum Jumps in the Non-Hermitian Dynamics of a Superconducting Qubit, *Phys. Rev. Lett.* **127**, 140504 (2021).
- [41] C. H. Bennett, H. J. Bernstein, S. Popescu, and B. Schumacher, Concentrating partial entanglement by local operations, *Phys. Rev. A* **53**, 2046 (1996).
- [42] C. M. Bender, D. C. Brody, and H. F. Jones, Complex Extension of Quantum Mechanics, *Phys. Rev. Lett.* **89**, 270401 (2002); **92**, 119902(E) (2004).
- [43] S. S. Bhosale, B. Rath, and P. K. Panigrahi, On Bell's inequality in PT-symmetric quantum systems, *Quantum Rep.* **3**, 417 (2021).
- [44] J. Wiersig, Review of exceptional point-based sensors, *Photonics Res.* **8**, 1457 (2020).